Journal of Materials Chemistry A

PAPER

View Article Online
View Journal | View Issue

Cite this: J. Mater. Chem. A, 2018, 6, 13062

Hexavalent chromium removal over magnetic carbon nanoadsorbents: synergistic effect of fluorine and nitrogen co-doping†

Jiangnan Huang,[a] Yuhang Li,[a] Yonghai Cao,*[a] Feng Peng,[ab] Yonggang Cao,[c] Qian Shao,[d] Hu Liu[e] and Zhanhu Guo*[f]

Received 28th March 2018
Accepted 30th May 2018

DOI: 10.1039/c8ta02861c

rsc.li/materials-a

Fluorine and nitrogen co-doped magnetic carbons (FN-MCs) were obtained through a facile pyrolysis–carbonization processes. The physical and chemical properties of FN-MCs were comprehensively studied by various characterization techniques. FN-MCs were applied as adsorbents for the removal of chromium(VI) ions from aqueous solutions. The adsorption performance and kinetic characteristics were evaluated in batch mode. The results showed that the FN-MCs displayed an enhanced removal efficiency in neutral solution, higher than solo N or F doped adsorbents. The highest removal capacity in both neutral and acidic solutions was 188.7 and 740.7 mg g^{-1}, respectively, competitive with the state-of-the-art carbon adsorbents. The unexpectedly high adsorption performance in the neutral solution can be attributed to the incorporation of the fluorine and nitrogen atoms simultaneously, which increased the negative charge density on the surface of the adsorbent. The removal efficiency increased along with the content of the heteroatoms and the defect value. The density functional theory (DFT) calculations demonstrated that the F and N co-doping reduced the adsorption energy between the Cr(VI) ions and adsorbent, thus boosting the adsorption efficiency in the neutral solution. Furthermore, the FN-MCs showed high stability in recycling tests for Cr(VI) removal.

1. Introduction

Heterogeneous atom dopants, such as nitrogen, fluorine and sulfur, in carbon-based materials ameliorate electronic features and provide rich functional groups, which are highly relevant to the active performance in a wide range of applications, including energy storage materials,[1] photocatalysts,[2] electrocatalysts,[3] heterogeneous catalysts,[4] environmental remediation,[5–7] *etc.* Su and co-workers found that phosphorous doped carbon nanotubes can be used as efficient catalysts for the oxidative dehydrogenation of *n*-butane and believe that the surface functionality is responsible for the activation of hydrocarbons.[8,9] Yu *et al.* found that nitrogen, phosphorous and boron doping can tune the catalytic activity in selective oxidation.[10,11] Gao *et al.* reported that nanocarbons can achieve a ultrahigh volumetric capacitance after fluorine and nitrogen co-doping.[12] The defect sites and surface chemistry were believed to play a significant role in their performance.[13,14] Recently, heteroatom doped carbon-based materials were discovered to be excellent adsorbents for heavy metal removal from aqueous solutions.[5,15]

Heavy metal pollution has become an urgent issue for our society caused by the rapid industrialization.[16] Cr(VI) is a typical contaminant because of its wide industrial application. It is crucial to remove Cr(VI) ions from waste water due to its high toxicity and mobility.[17] Adsorption was considered as a conventional and effective process because of its simple operation without producing by-products.[18,19] Typical adsorbents have been developed to improve the removal efficiency, such as clay minerals, biosorbents, zeolites, metal phosphates, activated carbon and magnetic carbons.[20–27] Among these adsorbents, magnetic carbons have become more popular due to their highly porous structure with easily controlled chemical properties and magnetization for easy separation.[19,25,26,28–31] In fact, waste water containing chromium discharged from the leather industry is usually acidic (see Table 4), and various studies were

[a]School of Chemistry and Chemical Engineering, Guangdong Provincial Key Lab of Green Chemical Product Technology, South China University of Technology, Guangzhou, Guangdong, 510640, China. E-mail: meyhcao@scut.edu.cn; Tel: +86 20 87114916

[b]School of Chemistry and Chemical Engineering, Guangzhou University, Guangzhou, Guangdong, 510006, China

[c]South China Sea Marine Engineering Surveying Center, State Oceanic Administration, Guangzhou, 510300, China

[d]College of Chemical and Environmental Engineering, Shandong University of Science and Technology, Qingdao 266590, China

[e]National Engineering Research Center for Advanced Polymer Processing Technology, Zhengzhou University, Zhengzhou 450002, China

[f]Integrated Composites Laboratory (ICL), Department of Chemical and Biomolecular Engineering, University of Tennessee, Knoxville, TN 37996, USA. E-mail: zguo10@utk.edu; Tel: +1 865 974 2933

† Electronic supplementary information (ESI) available: The additional characterization of the doped magnetic carbons. See DOI: 10.1039/c8ta02861c

conducted under acid conditions as well. Meanwhile, a pH adjustment with lime prior to this type of separation procedure was under consideration due to the process, cost and sludge treatment in this process. Recently, nitrogen doped magnetic carbons were proved to be an efficient adsorbent for heavy metal removal since the nitrogen dopant can adjust the electron density on the carbon surface.[5] The adsorption onto nitrogen doped magnetic carbon composites occurs through a chemical process involving valence forces. The Cr(III) adsorption capacity of nitrogen doped magnetic carbons was 10 times higher than that of active carbons.[32] Our previous work also demonstrated that the introduction of heteroatom dopants (N, F, *etc.*) can efficiently increase its negative charge density and simultaneously increase the adsorption ability for Cr(VI) and produced Cr(III) ions.[13,14] Hence, doping with two or more kinds of heteroatoms, such as nitrogen, fluorine, and sulphur, can afford a much more negative charge density on the material surface, which may be more favorable for metal adsorption. More recently, fluorine and nitrogen co-doped carbons gradually attracted attention in the scientific community, since fluorine atoms have more electronegativity than nitrogen and carbon atoms, displaying a much stronger ability to modulate the negative density charge on the adsorbent surface,[33–35] thus further enhancing its electron transfer properties. Doping with two kinds of heteroatoms into a carbon skeleton is believed to endow the material surface with distinguished electronic features, which could be more favorable for the adsorption of metal ions.[5,12,36] However, most studies showed that fluorine and nitrogen co-doped carbons have been only intensively studied in the field of electrochemistry, due to the strong ability to modulate the negative density charge on the carbon surface.[32] Li and co-workers found that fluorine and nitrogen co-doped graphene displayed a good performance in the oxygen reduction reaction, comparable with the-state-of-the-art Pt/C catalyst in an alkaline medium.[35] Gao *et al.* reported that fluorine and nitrogen co-doping endowed nanocarbons with high capacitance and stability in electrochemistry and believed that the fluorine doping could have an acidic character, acting as electron acceptors, while the nitrogen doping generally provided basic characteristics with electron-donor properties.[12] These results demonstrated that fluorine and nitrogen co-doping would provide unique properties for nanocarbons. Inspired by the aforementioned work, we aimed at synthesizing the two kinds of heterogeneous atom doped magnetic carbons with a high performance and stability in Cr(VI) removal. To the best of our knowledge, this is the first time to prepare the two kinds of heteroatom co-doped magnetic carbons for environmental remediation.

In this study, the fluorine- and nitrogen-codoped magnetic carbons (FN-MCs) were synthesized through a simple one step thermal pyrolysis method by using polyvinylidene fluoride (PVDF) and melamine as F and N precursors without post-processing, and utilized as adsorbents for Cr(VI) removal. The comprehensive characterization of the chemical and physical properties of these carbon adsorbents was performed. The adsorption performance and mechanism were carefully studied. The density functional theory (DFT) calculation was applied to help us to understand the inner removal mechanism over the co-doped magnetic carbon.

2. Experimental section

2.1 Materials

Potassium dichromate (99%, $K_2Cr_2O_7$), ethanol (99.9%), 1,5-diphenylcarbazide (97%, DPC) and denatured ethyl alcohol (92.2%) were purchased from Alfa Aesar Company. Sodium hydroxide (NaOH, 99.1%), $Fe(NO_3)_3\cdot 9H_2O$ (99%), sulfuric acid (H_2SO_4, 95%), polyvinylidene fluoride (PVDF, 99%), phosphoric acid (H_3PO_4, 85 wt%) and melamine (99%) were obtained from Fisher Scientific Co. Ltd. All the chemicals were used as received without any further purification.

2.2 Synthesis of doped magnetic carbon nanoadsorbents

The magnetic carbon nanoadsorbents were prepared as follows: typically, the FN-MCs were synthesized as follows: 3 g mixtures of melamine and PVDF at mass ratios (based on the weight of PVDF) 0%, 33%, 50%, 66, 80%, 100% and 6 g $Fe(NO_3)_3\cdot 9H_2O$ were added to an ethyl alcohol solution, and then the mixtures were treated under ultrasonication for 2 h. After that, the mixtures were dried at 110 °C overnight. The obtained solid samples were then carbonized at 800 °C for 2 h under a N_2 atmosphere. The obtained carbon samples can be identified as FN-MC-0, FN-MC-33, FN-MC-50, FN-MC-66, FN-MC-88 and FN-MC-100, respectively.

2.3 Characterization

Brunauer–Emmett–Teller (BET) specific surface areas were measured by N_2 adsorption at liquid N_2 temperature using an ASAP 2010 analyzer. Raman spectra were obtained using a Lab-RAM Aramis micro Raman spectrometer with an excitation wavelength at 630 nm with 2 mm spot size. Scanning electron microscope (SEM) images were obtained with a FEI Quanta 600F electron microscope. Transmission electron microscope (TEM) images were obtained with a FEI Tecnai G2 12 microscope which was operated at 100 kV and a high resolution TEM (Techni F20) with a double tilt holder operating at an emission voltage of 200 kV. The specimens for TEM were prepared by ultrasonically suspending the sample in acetone and depositing a drop of the suspension onto a grid. X-ray photoelectron spectroscopy (XPS) was performed using a Kratos Axis Ultra (DLD) spectrometer equipped with an Al Kα X-ray source in an ultrahigh vacuum (UHV) ($<10^{-10}$ Torr). The binding energies (±0.2 eV) were referenced to the C_{1s} peak at 284.6 eV. The surfaces of the samples were cleaned by heat treatment at 100 °C in UHV prior to the measurements. X-ray diffraction (XRD) patterns were recorded on a Bruker D8 ADVANCE diffractometer equipped with a rotating anode using Cu Kα radiation (40 kV, 40 mA). The magnetic property measurements were carried out using a 2 T physical property measurement system (PPMS) by Quantum Design at room temperature. Thermogravimetric analysis (TGA) was conducted using a TA Instruments Q-500 at a heating rate of 10 °C min^{-1} and an air flow rate of 20 mL min^{-1} from 25 to 800 °C.

A Mössbauer spectrometer was set to produce a high-precision Doppler velocity modulation of the source γ radiation. The effects of the Doppler velocity modulation on the absorption of γ radiation were recorded synchronously in the 1024 channels of a multichannel analyzer. The result was 1024 numbers representing registered gamma quanta (representing a singular quantum) passing through the absorber under the condition of different Doppler velocities. A separate calibration procedure was used to establish the exact correspondence channel-velocity (spectrometer calibration was performed by measuring a standard α-Fe absorber, which produces a well-known six line spectrum. The whole velocity range was calibrated using these six velocity points). The shape of the absorption spectrum was fitted to a theoretical model line shape, which was a superposition of singlets, doublets and sextets (^{57}Fe case) of a Lorentzian form. The result was investigated using the chi^2 criterion and the theoretical line shape was tailored to fit the experimental spectrum by the adjustment of spectral parameters like isomer shift, quadrupole splitting, hyper fine magnetic field, and so on.

2.4 Cr(VI) removal

Typically, the FN-MCs were added to the Cr(VI) solution and treated under ultrasonication for a certain time at room temperature. Cr(VI) removal efficiency based on the effects of different Cr(VI) concentrations (from 1.0 to 320 mg L^{-1}), nanoadsorbent doses (from 0.5 to 5 g L^{-1}), treatment times (from 0 to 15 min) and pH values (from 1.0 to 13, measured with a pH meter, Vernier Lab Quest with a pH-BTA sensor) was investigated in detail in this experiment. HCl (1 mol L^{-1}) and NaOH (1 mol L^{-1}) solutions were used to adjust the solution pH value. For the kinetic study, the synthesized magnetic carbons were used to treat different concentrations of Cr(VI) solution with the initial pH at 1.0 and 7.0, respectively. In order to make sure that the adsorbent was dispersed in the solution fully and quickly, the suspension liquid with adsorbents was treated under ultrasonication (300 W, KQ-300DE, Kunshan Ultrasonic Instrument Co., LTD) at room temperature. And the rated power was set accordingly since it has a strong influence on the Cr(VI) removal efficiency.[37,38] The Cr(VI) concentrations that remained in solutions were measured at different time intervals. The Cr(VI) concentration in solution was measured by the colorimetric method based on our earlier publications.[13,14]

2.5 Computational methods

The adsorption properties were investigated by spin-polarized DFT calculations with the DMol3 package.[39] Exchange–correlation functions were described by GGA/PBE.[40] The electronic basis set was a double numerical plus polarization (DNP) set, which is equal to 6-31G** in Gaussian. The "DFT semi-core pseudopods (DSPPs)" method was adopted as the core treatment.[41] The orbital cutoff with 5.0 Å was set for all atoms. To avoid the shortage of handling weak interactions by DFT, the long range dispersion was corrected by using the Grimme scheme.[42,43] The conductor-like screening model (COSMO) with a permittivity of 78.54 was considered to mimic structures encased by the aqueous layer.[44] It is essential to extract a simplified model as the initial structure in DFT calculations. The surface of the nanomaterial synthesized in this contribution basically consists of graphitic carbon atoms. The partial surface, referring to the adsorption location for Cr(VI), can be treated as a planar structure. Thus, the graphene model was adopted in calculations. The primitive hexagonal graphene cell was extended to a (4 × 4 × 1) supercell with the optimized parameters of 9.84 Å × 9.84 Å × 25 Å, where the extension along the *c* axis represented the elimination of interactions between adjacent layers. The *k*-point was set to 8 × 8 × 1 after convergence tests. We assumed that Cr(VI) exists as a form of CrO_4^{2-} clusters with two negative charges in the neutral solution. The adsorption energy E_{ads} was calculated according to the formula as below:

$$E_{ads} = E(X\cdots CrO_4^{2-}) - E(X) - E(CrO_4^{2-}) \quad (1)$$

where $E(X\cdots CrO_4^{2-})$ is the energy of the steady adsorption state on different adsorbents; $E(X)$ is the energy of the isolated adsorbent; $E(CrO_4^{2-})$ is the energy of the isolated adsorbate CrO_4^{2-} cluster with two negative charges.

3. Results and discussion

3.1 Textural properties

Fig. 1a and b show the typical granulated structure of the FN-MCs, where the iron or iron oxides were encapsulated by carbon layers with about 3 nm thickness. This structure was similar to that of solo F or N doped magnetic carbons (Fig. S1†).[13,14] HRTEM results demonstrated that a lattice fringe of 2.03 Å was obtained for the core component, corresponding to the (110) plane of Fe^0 particles, while the lattice fringe of 2.35 Å in the left upper corner indicated the (111) plane of FeF_2. The aggregation of the iron oxide nanoparticles probably occurred during the carbonization leading to non-uniform particle sizes of about 30–120 nm.[19] Bulged and wrinkled graphene sheets were observed on the carbon surface of FN-MCs, offering a high surface area and lots of active open-edge sites.[34] The uniform distribution of N and F elements was observed (Fig. 1c), which was also observed in the XPS results (Fig. 1d and Table S1†), demonstrating that the introduction of N and F atoms into the carbon skeleton was achieved. Meanwhile, the Fe element was observed spread all over the surface of the carbon nanocomposites. XRD and Mössbauer results further revealed that metallic irons existed on the surface (Fig. 1e, 2 and Table 1), due to the reduction reaction with carbons during the calcination at 800 °C.[19] A large number of FeF_2 nanoparticles were synthesized over F containing samples in this procedure, attributed to the pyrolysis reaction between the FeO_x and PVDF.[45]

Raman spectral results of FN-MCs are shown in Fig. 1f and Table S2.† The nitrogen and fluorine atom doping enables extremely broadened peaks, demonstrating that the disorder degree (I_D/I_G) of the graphene layer was greatly enhanced after the F and N doping.[34] In this study, 5 peaks, *i.e.*, *I* (1170 cm^{-1}), D (1320 cm^{-1}), D″ (1490 cm^{-1}), G (1560 cm^{-1}), and D′ (1640 cm^{-1}), were deconvoluted with an appropriate Lorentzian–Gass ratio.

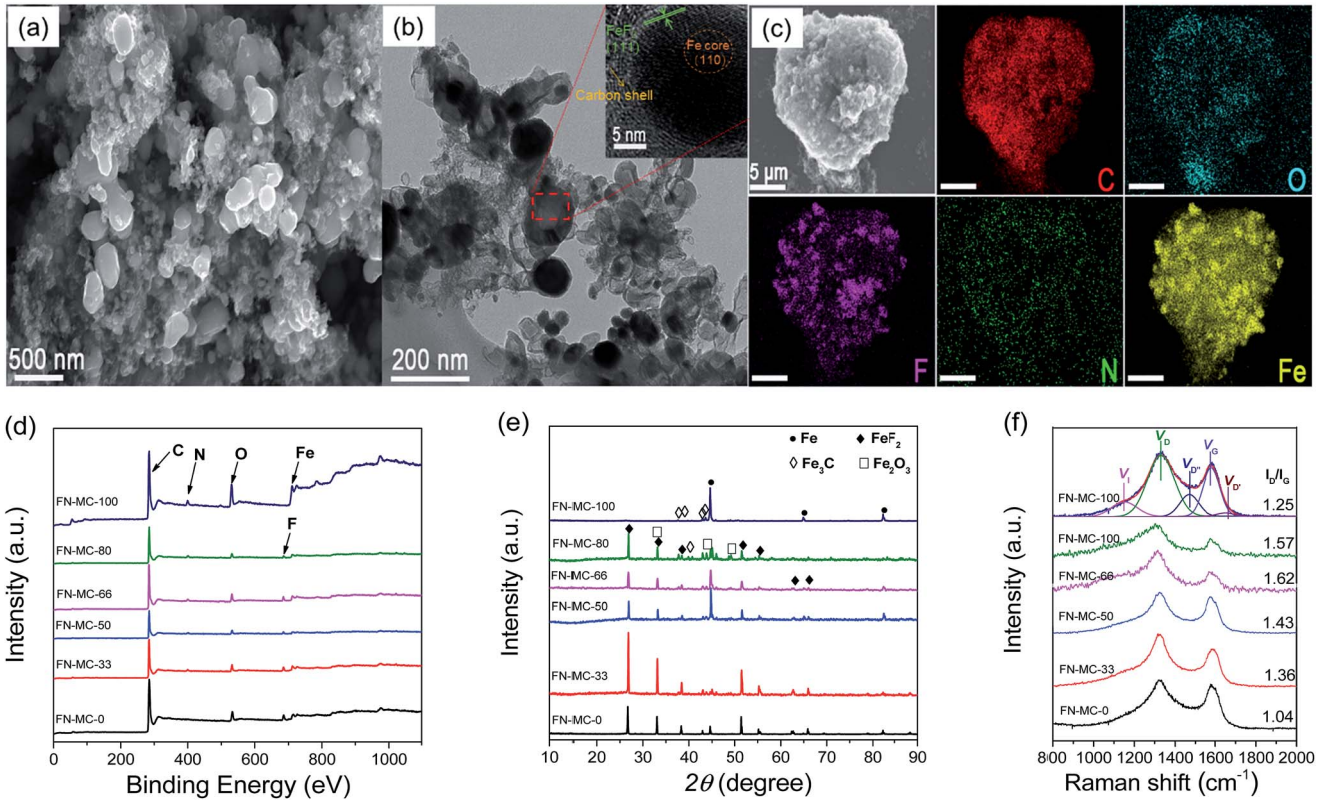

Fig. 1 Typical morphology and element distribution of FN-MCs, (a) SEM and (b) TEM and HRTEM images, (c) SEM image and the corresponding EDS elemental mappings, carbon (red), oxygen (blue), fluorine (purple), nitrogen (green) and iron (yellow). (d) XPS survey, (e) XRD patterns and (f) Raman spectra of the FN-MCs used in this work.

The intensity ratio of D to G band (I_D/I_G) was used to evaluate the defective degree of FN-MCs.[46] The widening and overlapping of G and D bands of the samples can be attributed to the enhanced vibrations from *I*, D″ and D′ bands.[47] The I_D/I_G value increased from 1.09 to 1.62 firstly (FN-MC-0 to FN-MC-66) and then declined to 1.21 (FN-MC-66 to FN-MC-100) along with the addition of melamine dosage in the precursor. The FN-MC-66 has the highest I_D/I_G value at 1.62. These results demonstrated that the defects and distortions over the FN-MCs can be tuned by modifying the ratio of fluorine and nitrogen dopants into the carbon skeleton.[34]

The surface chemistry of the FN-MCs was investigated by XPS. According to Table S1,† the N content increased from 0 to 4.28 at% with the melamine dosage increasing in the precursor, while the F content decreased from 0 to 2.46 at%. To provide an intrinsic insight into the effect of F and N doping in this work, the high-resolution N 1s and F 1s spectra of the doped magnetic carbons were obtained. For the N 1s spectra, five peaks were fitted at 398.3, 399.9, 401.04, 403.0 and 405.0 eV, which were assigned to pyridinic N (N1), pyrrolic N (N2), graphitic N (N3), pyridine-*N*-oxide (N4) and C–O–N (N5), respectively (Fig. 3a and Table S3†).[46,48] The high-resolution F 1s spectra of the doped magnetic carbons were fitted to four peaks, centered at about 684.8, 685.8, 687.3 and 689.2 eV, corresponding to FeF_2 (F1), ionic C–F(F2), semi-ionic C–F (F3) and covalent C–F (F4), respectively (Fig. 3b and Table S4†).[45,49–51] The gross heteroatom and functionality contents are summarized in Fig. 4. In this study, the N content changed slightly according to the variation of the melamine amount in the precursor, and pyridinic, pyrrolic and graphitic N were observed as the dominant components for the N doping. For the F doping, the F content could be tuned significantly when the PVDF loading varied, while the functionalities FeF_2, ionic and semi-ionic C–F were found to be the major components.

3.2 Cr(VI) removal

The textural properties of FN-MCs (see Fig. S2 and Table S5†) and their Cr(VI) removal performance in the neutral solution are summarized in Table 2. The solely F doped magnetic carbons (FN-MC-0) showed a comparatively low efficiency, 43.4%, in the Cr(VI) removal. The Cr(VI) removal activity increased when the N content increased at the beginning (Table S1†). The FN-MC-66 displayed the best performance (92% Cr(VI) removal percentage). However, continuing to increase the N doping would lead to the decrease of Cr(VI) removal efficiency, and might be due to the decrease of the content of the F dopant in the adsorbent. FN-MC-100 showed the lowest activity, 24.7% removal percentage, ascribed to the solely N doping in this carbon adsorbent. These results demonstrated that the F and N co-doped carbon adsorbents can achieve a higher removal performance. In the case of the carbon adsorbent, the adoption rate normalized by adsorbent weight or area is a very

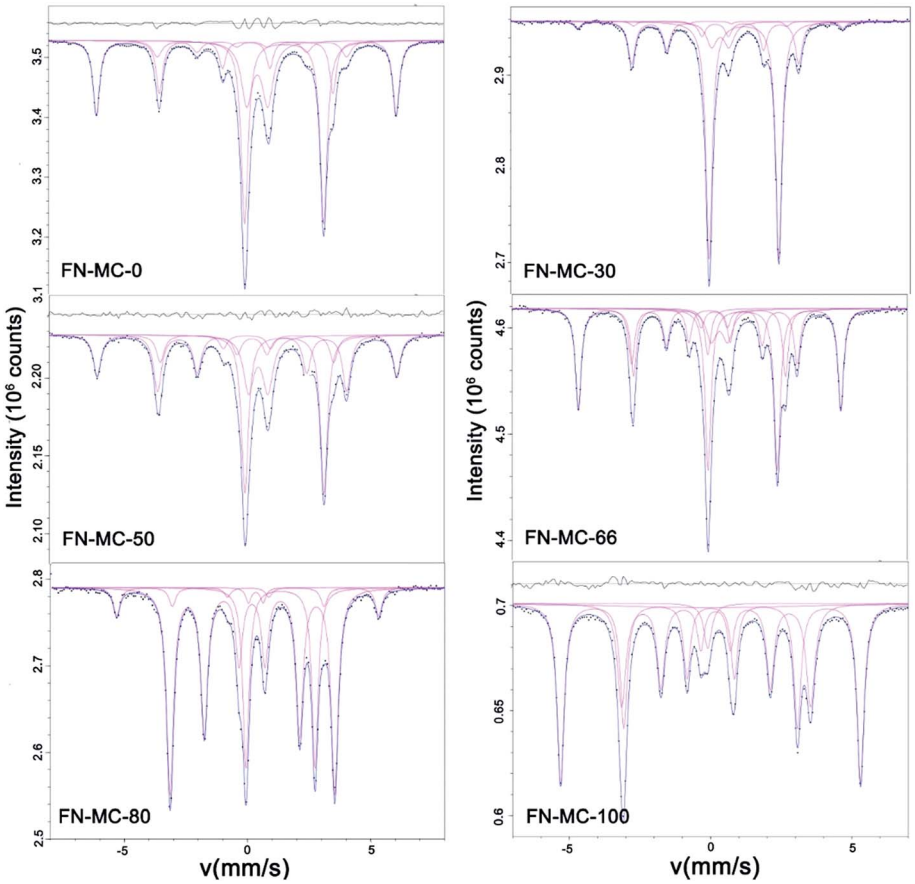

Fig. 2 Mössbauer spectra of FN-MCs used in this work.

important parameter.[13,14] Therefore, we defined that the removal rate is the Cr(VI) removal efficiency normalized by the adsorbent weight (r_g) and specific surface area (r_s). In this work, similar to the Cr(VI) removal percentages, the Cr(VI) removal rate firstly increased and then decreased with the N content increasing. Adsorption capacities as high as 20.69 mg g^{-1} min^{-1} and 0.250 mg m^{-2} min^{-1} were obtained in the Cr(VI) removal in the neutral solution. These results demonstrated that there is a synergistic effect between the F and N dopants, enhancing the removal of Cr(VI) ions.[12,36]

Based on the aforementioned results, the FN-MC-66 was proved to be the best adsorbent. The effects of parameters such as Cr(VI) concentration, adsorbent dose, treatment time and pH on the Cr(VI) removal efficiency of FN-MC-66 were then investigated carefully (Fig. 5). In this study, up to 175 mg g^{-1} Cr(VI) can be totally removed by the adsorbent with 2.5 g L^{-1} dosage. The removal percentage then decreased from 200 mg g^{-1}, due to the limited active sites (Fig. 5a). When the Cr(VI) concentration was 320 mg g^{-1}, up to 75% Cr(VI) ions were still removed; meanwhile the q_t was as high as 97 mg g^{-1} in the neutral solution. By increasing the adsorbent dose to 3.5 g L^{-1}, 320 mg g^{-1} Cr(VI) was completely removed within 10 min (Fig. 5b). As the treatment time was prolonged, the Cr(VI) removal percentages increased, whereas the removal capacity gradually became lower, since the adsorption tended to be saturated. The Cr(VI) removal rate and adsorption isotherms were also investigated. As shown in Fig. 5c, a rapid removal performance, 2.5 min for 64.7% Cr(VI) removal at 320 mg g^{-1} (initial Cr(VI) concentration), was obtained firstly, and then the removal rate became slower, indicating that the adsorption is gradually saturated and the surface of the adsorbent is covered by Cr(VI) ions and as-reduced Cr(III) ions.[5,19] The pH value has a significant effect on the Cr(VI) removal efficiency (Fig. 5d). We adjusted the pH value ranging from 1.0 to 13. Acid medium in the solution usually can greatly improve the removal of Cr(VI).[19,52] In this work, Cr(VI) with a concentration of 1000 mg g^{-1} was totally removed at pH lower than 2, and then the removal activity decreased from 3 (pH value). These results may be attributed to the redox of $HCrO_4^-$ as well as the electrostatic attraction between the Cr(VI) ions and magnetic carbons, which also can be enhanced by the fluorine

Table 1 Room-temperature Mössbauer spectral data of the FN-MCs

Adsorbent	Metallic iron	Cementite Fe_3C	Fe^{2+}	Fe^{3+}
FN-MC-0	31	10	39	20
FN-MC-33	4	24	62	10
FN-MC-50	39	21	30	10
FN-MC-66	20	28	34	18
FN-MC-80	8	65	25	2
FN-MC-100	50	32	8	10

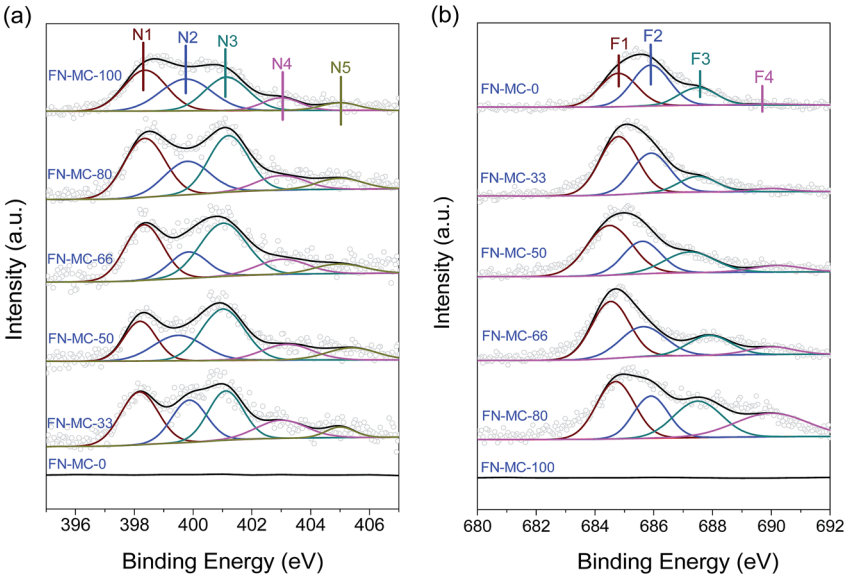

Fig. 3 N_{1s} (a) and F_{1s} (b) XPS spectra of the FN-MCs used in this work: pyridinic N (N1), pyrrolic N (N2), graphitic N (N3), pyridine-*N*-oxide (N4), C–O–N (N5), FeF_2 (F1), ionic C–F (F2), semi-ionic C–F (F3) and covalent C–F (F4), respectively.

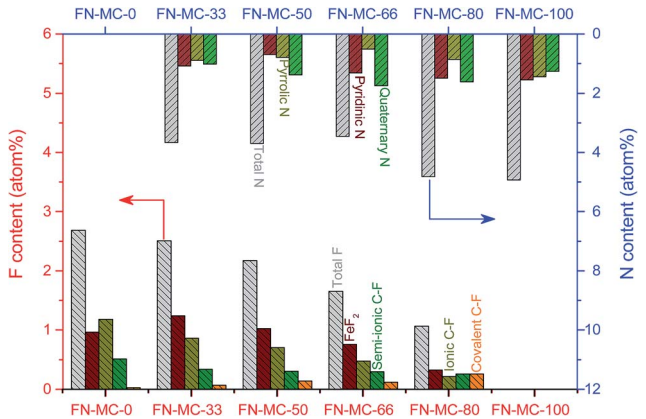

Fig. 4 Distribution of the N and F functionalities of FN-MCs used in this work.

and nitrogen dopants.[5,15] The introduction of N or F doping can decrease the pH_{zc},[13,14] enhancing the adsorption ability of FN-MCs. The apparent adverse influence of the basic medium was also observed with the pH ranging from 8 to 13. Only 7.0% Cr(VI) removal percentage was obtained when the pH value is 13, which can be attributed to the adsorption competition between the high OH^- concentration and Cr(VI) ions on the adsorbent surface.[14]

3.3 Adsorption kinetics and isotherm

From the aforementioned results, Cr(VI) ions can be removed rapidly with the FN-MC-66 adsorbent. Two typical models, *i.e.*, pseudo-first-order and pseudo-second-order models, were utilized to evaluate the Cr(VI) removal kinetics in the current study. As can be seen from Fig. S3,† the removal process was found to be favorable as the pseudo-second-order models with a high correlation coefficient at 0.99, indicating that the Cr(VI) removal by FN-MC-66 was a chemical adsorption, which was consistent with our earlier publications.[13,14,53]

For the adsorption isotherm, the Langmuir and Freundlich models are generally used to elaborate the adsorption mechanism.[19,26,29] In this study, the relationship between the removal ability of the material and the concentration of the contaminant

Table 2 Physical properties and performance of magnetic carbon in Cr(VI) removal[a]

Entry	Adsorbent	S_{BET}[b] ($m^2\ g^{-1}$)	X[c] (%)	r_g[d] ($mg\ g^{-1}\ min^{-1}$)	r_s[e] ($mg\ m^{-2}\ min^{-1}$)
1	FN-MC-0	124.6	43.4	9.29	0.075
2	FN-MC-33	121.9	52.5	11.26	0.093
3	FN-MC-50	97.9	66.2	14.19	0.145
4	FN-MC-66	82.7	96.6	20.69	0.250
5	FN-MC-80	62.8	45.2	9.68	0.154
6	FN-MC-100	56.2	24.7	5.28	0.094

[a] Conditions: [Cr(VI)] = 200 mg L^{-1}, pH = 7.0, adsorbent dosage: 2.5 g L^{-1}, and treatment time: 10 min. [b] The information of BET surface area, pore size and pore volumes can be seen in Fig. S3 and Table S5. [c] X: removal percentage. [d] Removal rate of Cr(VI) per gram of adsorbent based on the treatment for 2.5 min. [e] Removal rate of Cr(VI) per m^2 of adsorbent surface based on the treatment for 2.5 min.

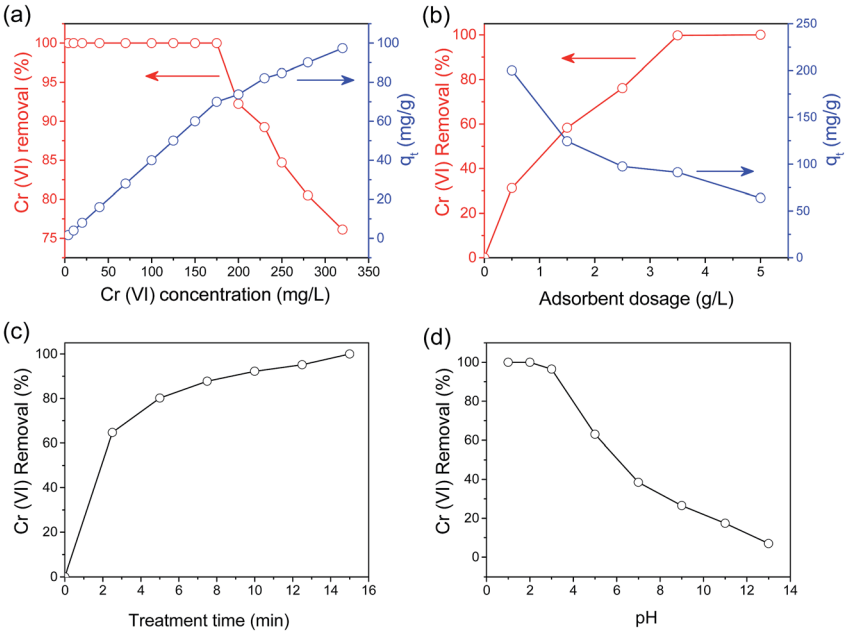

Fig. 5 (a) Effect of initial Cr(VI) concentration on Cr(VI) removal performance (adsorbent dosage: 50.0 mg, volume: 20 mL, pH: 7.0, treatment time: 10 min) and the transformed rate plot C_e *vs.* q_t (open circle with blue color); (b) Cr(VI) removal performance for different adsorbent concentrations ([Cr(VI)] = 320 mg L^{-1}, pH = 7.0, adsorbent dosage: 50.0 mg, volume: 20 mL, treatment time: 10 min); (c) Cr(VI) removal performance with different treatment times ([Cr(VI)] = 200 mg L^{-1}, pH = 7, adsorbent dosage: 50.0 mg, volume: 20 mL); (d) effect of pH on the Cr(VI) removal performance (adsorbent dosage: 50.0 mg, volume: 20 mL, pH = 7.0, treatment time: 10 min).

solution was illustrated. The Langmuir isotherm was described as the following equation:

$$\frac{C_e}{q_e} = \frac{1}{bq_{max}} + \frac{C_e}{q_{max}} \quad (2)$$

The Freundlich isotherm is an empirical model that considers heterogeneous adsorptive energies on the surface of the absorbent and can be described as the following equation:

$$\log q_e = \log k_f + \frac{1}{n}\log C_e \quad (3)$$

where C_e (mg L^{-1}) is the equilibrium Cr(VI) concentration, q_e (mg g^{-1}) is the Cr(VI) amount adsorbed at equilibrium, q_{max} (mg g^{-1}) is the adsorption capacity of adsorbents, and b, k_f and n are constants.

Fig. S4† shows the adsorption isotherms of Cr(VI) for the FN-MC-66. The Langmuir and Freundlich models were used to fit the adsorption behavior (Table 3). The excellent fitted results, with correlation coefficients of 0.992 and 0.987 for the Langmuir and Freundlich models, respectively. The maximum adsorption capacity (q_{max}) of FN-MC-66 was found to be 188.7 mg g^{-1} in the neutral and acid solutions respectively, which is much higher than that of other adsorbents in the neutral solution (Table 4). For the acid solution, the q_{max} of FN-MC-66 was 740.7 mg g^{-1}, which is competitive with the state-of-the-art carbon adsorbents. The q_{max} of the solely N and F doped carbons was higher than that of FN-MC-66 in the acid solution, due to the higher content of Fe^0 and Fe^{2+} particles (Fig. S5†), which were the important reductants for the Cr(VI) reduction.[14] The adsorption capacity per m^2 of the adsorbent surface (q_s) is another important property for adsorbents.[13,14] In this work, the q_s of FN-MC-66 was 2.283 and 8.96 mg m^{-2} in the neutral and acid solutions, much higher than those of other adsorbents. These results demonstrated that the FN-MC-66 can be used as an alternative adsorbent for heavy metal removal from wastewater.

Table 3 Isotherms and kinetic parameters for the adsorption of chromium on FN-MC-66

	Langmuir			Freundlich		
pH	q_{max} (mg g^{-1})	b	R^2	n	k_f	R^2
7	188.7	0.0033	0.992	1.84	0.453	0.987
1	740.7	0.0043	0.951	1.03	0.424	0.992

3.4 Stability

The recyclability of an adsorbent is very important for its commercial application by reducing the overall cost. In this work, we selected the FN-MC-66 as the adsorbent with 200 mg g^{-1} Cr(VI) initial concentration in neutral solution for the reusability study. After each adsorption, the adsorbent was washed with deionized water and 0.01 M NaOH solution for the regeneration.[54,55] As shown in Fig. 6a, the FN-MC-66 possessed more than 80.7% Cr(VI) removal capacity after 5 cycles. The removal capacity q_t was 64.5 mg g^{-1}. A slight loss of the removal activity was observed, as a result of the consumption of metallic iron and the blocking of active sites. Significant decreases were observed in the

Table 4 Comparison of Cr(VI) adsorption capacities with other adsorbents

	Adsorbent	S_{BET} (m^2 g^{-1})	q_{max}[a] (mg g^{-1})	q_s[b] (mg m^{-2})	pH	Ref.
Neutral solution	FN-MC-66	82.7	188.7	2.28	7	This work
	N-MC	56.2	29.46	0.52	7	13
	F-MC	121.6	48.78	0.40	7	14
	Magnetic carbon (cellulose)	111.4	15.3	0.14	7	19
	MN (cotton fabric)	91.1	3.74	0.04	7	26
	Graphene nanocomposites	42.1	1.03	0.02	7	58
Acid solution	FN-MC-66	82.7	740.7	8.96	1	This work
	N-MC	56.2	2001.4	35.61	1	13
	F-MC	121.6	1423.4	11.71	1	14
	MRT	628.0	102.88	0.16	3	63
	Activated carbon	n/a	112.36	n/a	1	64
	MnO_2/Fe_3O_4/o-WCNTs	92.0	186.9	2.03	2	54
	α-Fe_2O_3	40.0	4.47	0.11	3	52
	N doped porous carbon (Fe)	1136.0	16	0.02	3	5
	N-doped porous carbon (Ni)	2148.4	96.27	0.04	2.5	65
	Micron Fe	—	2.16–1.33	—	3	66
	Nano-Fe	35	64.16–67.67	1.83–1.93	3	66
	CNT core-in-hematite shell capsules	270	29.16	0.1	5	67
	PAN-NH_2 nanofibers	—	137.6	—	2	68
	PEI-modified aerobic granular sludge	—	348.1	—	5.2	69
	MRT	628.0	102.88	16.4	3	63
	Surface functionalized PAN fiber	—	20.7	—	2.5	70
	Surface modified tannery residual biomass	—	177–217	—	2	71
	Activated carbon	—	112.36	—	1	64

[a] q_{max} is obtained through the Langmuir isotherm model. [b] q_s represents the adsorption capacity per m^2 of adsorbent surface.

magnetization and TGA of the used adsorbent (Fig. 6b and c), demonstrating that the iron was consumed by Cr(VI) ions through the redox reaction.[19] The peaks centered at 576.9 and 586.6 eV are associated with Cr(III), and the peaks at 578.9 and 588.7 eV are attributed to the presence of Cr(VI). The XPS analysis indicates that Cr is adsorbed as Cr(III) and Cr(VI), suggesting that some of the adsorbed Cr(VI) anions were reduced to Cr(III) before depositing on the surfaces of the adsorbent.[5] Meanwhile Cr(VI) and the as-produced Cr(III) ions were tightly adsorbed on this surface of the adsorbent (see Fig. 6d and S6†). These results demonstrated that FN-MC-66 has a good reusability for Cr(VI) removal and also evidenced

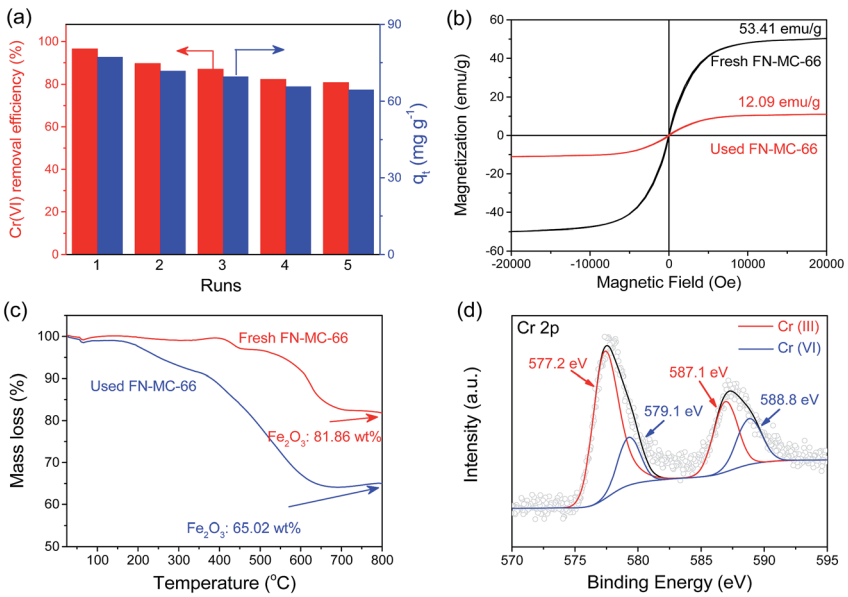

Fig. 6 (a) Reusability of FN-MC-66 for Cr(VI) removal in neutral solution. (b) Room temperature magnetic hysteresis loops of the fresh and used magnetic carbons. (c) The TGA curve of the fresh and used FN codoped magnetic carbons from 25 to 800 °C in air atmosphere with a heating rate of 10 °C min^{-1}. (d) Cr_{2p} XPS spectra of the recycled FN-MC-66.

that the fluorine and nitrogen atoms can efficiently maintain the Cr(VI) removal stability.

Additionally, to investigate the removal efficiency of FN-MC-66 in the presence of different ions, several types of ions with 200 mg L^{-1} concentration were added to the solution and the variation of the performance was observed (Fig. S7†). The cations, such as Na^+, Fe^{3+}, Zn^{2+}, Pb^{2+}, Cu^{2+}, *etc.*, were selected. Most of them displayed a negligible effect on the Cr(VI) removal. The anions, PO_3^{3-}, SO_4^{2-} and Cl^-, were added as well. The anions, SO_4^{2-} and Cl^- ions, showed no significant influence on the Cr(VI) removal except PO_3^{3-}. These results demonstrated that the FN-MC-66 in this study still could provide a good selectivity for Cr(VI) removal while most of the typical foreign ions existed, and the removal performance could be hindered in the presence of Na^+ and PO_3^{3-} ions.

3.5 Mechanism study

To investigate the mechanism of Cr(VI) removal over FN-MCs, the relationship between the Cr(VI) removal efficiency and the physical and chemical properties as well as the structure was discussed in detail. According to previous work, there is a chemical reduction reaction of Cr(VI) ions to nontoxic Cr(III) ions occurring in this system, which is very important for the Cr(VI) removal.[19,25,26,56,57] The zero-valent iron and Fe^{2+} ions play a significant role in the magnetic carbon–Cr(VI) removal system, since the low pH value can effectively improve the Cr(VI) removal, involving more H^+ in the system.[26,58] Nevertheless, very low removal performances were still obtained in the neutral solution or low pH solution (pH value at 2–3) with undoped magnetic carbons or solely nitrogen doped magnetic carbons as an adsorbent (Table 4). Therefore, there is a significant factor that can dramatically increase the Cr(VI) ion removal performance. From Table 1, the results evidently demonstrated that the activities of FN-MCs could be modulated by the mass ratio of melamine and PVDF, which means that the physical and chemical properties of FN-MCs will dramatically affect the adsorbent performance. These distinct activities of FN-MCs for Cr(VI) removal propelled us to find the intrinsic effects on the structure–performance relationship of the MCs with different heteroatom doping levels and architecture in Cr(VI) removal in the neutral solution. As the adsorption and redox occur on the surface of magnetic carbons, the surface-area-normalized removal rates were utilized to evaluate the removal performance in this study.

The magnetization of the magnetic adsorbent is not only beneficial for the withdrawal of the adsorbents, but also may be important for the adsorption of metal ions.[58] In the case of Cr(VI) removal, the Cr(VI) and as-synthesized Cr(III) ions can be adsorbed onto the surface of magnetic carbons due to electrostatic attraction. Is there any relationship between the magnetization and removal efficiency? Work focused on this issue has been rarely reported. In this work, the magnetic property of these carbon adsorbents was carefully measured (see Fig. S8 and Table S6†). The removal rate increased dramatically and then decreased along with the magnetization increasing (see Fig. S9†). Very narrow intervals were observed for the Cr(VI) removal rate, which indicated that the magnetization is not the elemental factor for the FN-MC performance, and a similar phenomenon was observed in graphene oxide based magnetic materials, in which Ppy–Fe_3O_4/rGO displayed better removal performance but has lower magnetization than Fe_3O_4/rGO.[59]

More recently, heteroatom doping is believed to increase the negative charge density and simultaneously increase the adsorption ability of the carbon adsorbent.[13,14] As mentioned by earlier publications, heteroatom functionalities play a significant role in the adsorption of heavy metals. We here correlated the Cr(VI) removal rate with the amount of fluorine and nitrogen functionalities. Although heteroatoms can indeed increase the removal efficiency, there is no monotonic relationship between the gross heteroatom content and the removal efficiency, as shown in Fig. S10.† The volcanic type curve indicated that the specific activity based on the two kinds of heteroatom dopants has a significant effect on promotion of the Cr(VI) removal. Also, the relationships between the content of the deconvoluted heteroatom functionalities and removal rate were investigated. A positive relationship between the removal rate and graphitic N was observed (Fig. 7a), demonstrating that graphitic N may be one of the most important active sites for the improvement of Cr(VI) removal. Meanwhile, the chaotic relationships between the removal rate with other functionalities (*i.e.*, pyridinic N, pyrrolic N and C–F bonds) demonstrated that the unique Cr(VI) removal efficiency cannot be simply attributed to certain heteroatom functionalities (Fig. S11 and S12†). According to the aforementioned results, the fluorine and nitrogen co-doped carbons (FN-MC-33, FN-MC-50, FN-MC-66 and FN-MC-80) displayed better removal efficiency than the solely heteroatom doped magnetic carbons (FN-MC-0 and FN-MC-100), indicating that there is a synergistic effect between the fluorine and nitrogen dopants on the Cr(VI) removal, thus facilitating the removal efficiency. Based on reported work, pyridinic N, pyrrolic N and C–F bonds universally emerge at defects such as vacancies, free edges, or domain boundaries.[11,60] Heterogeneous or carbon atoms exposed at the edges or vacancies are usually considered as the active sites in various fields due to their high density of electrons,[60,61] which reminds us that defect sites are also the significant active sites for the adsorption of Cr(VI) ions over FN-MCs. As shown in Fig. 7b, a positive effect of defects on the Cr(VI) removal rate of FN-MCs was observed, which demonstrated that the defect was a significant factor for the Cr(VI) adsorption, since lots of heteroatoms were dispersed at the defects. Therefore, we correlated the removal rate with the fluorine and nitrogen dopants at defects (including pyridinic N, pyrrolic N and all the C–F bond functionalities, see Fig. 7c). An excellent monotonic relationship was observed, strongly revealing the positive effect of the heterogeneous dopant at defects on the Cr(VI) removal.

3.6 Computational simulations

To further understand the intrinsic effect of F and N co-doping, DFT calculations were carried out to show the adsorption ability between the heteroatoms and Cr(VI) ions. According to the reported literature, heteroatom functionalities play a critical role

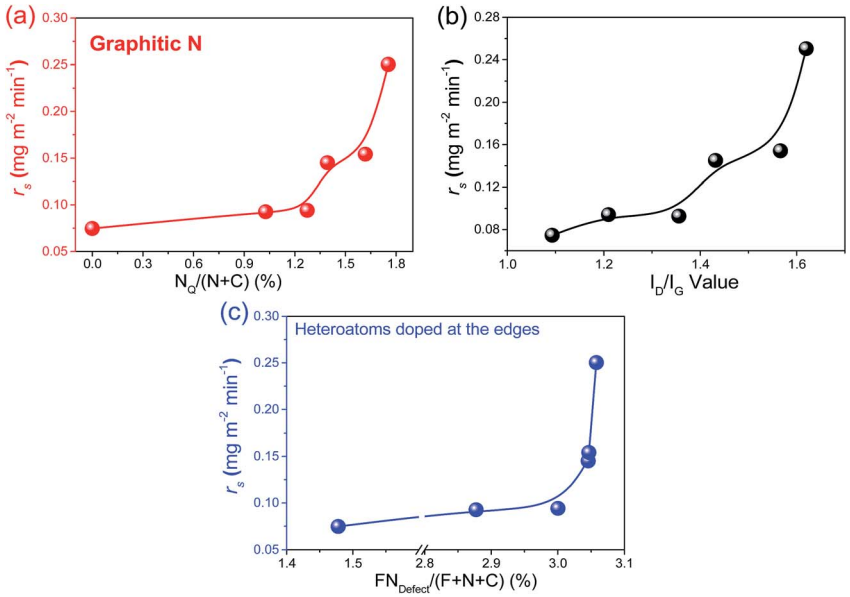

Fig. 7 Dependences of the Cr(VI) removal rate on the amounts of (a) the quaternary N, (b) the defects of FN-MCs and (c) the F and N dopants at the edges of carbons in this work.

in the adsorption of reactive species to improve the reaction.[9–11] In this study, CrO_4^{2-} ions were selected as the model ions, due to the existence of the Cr(VI) form in neutral solution.[19] The steady-state configurations between CrO_4^{2-} ions and adsorbents are shown in Fig. 8. One iron atom under the graphene plane was believed to be the adsorption location. The nitrogen and fluorine atoms were located near iron. It was noteworthy that the fluorine atom existed as two kinds of bond

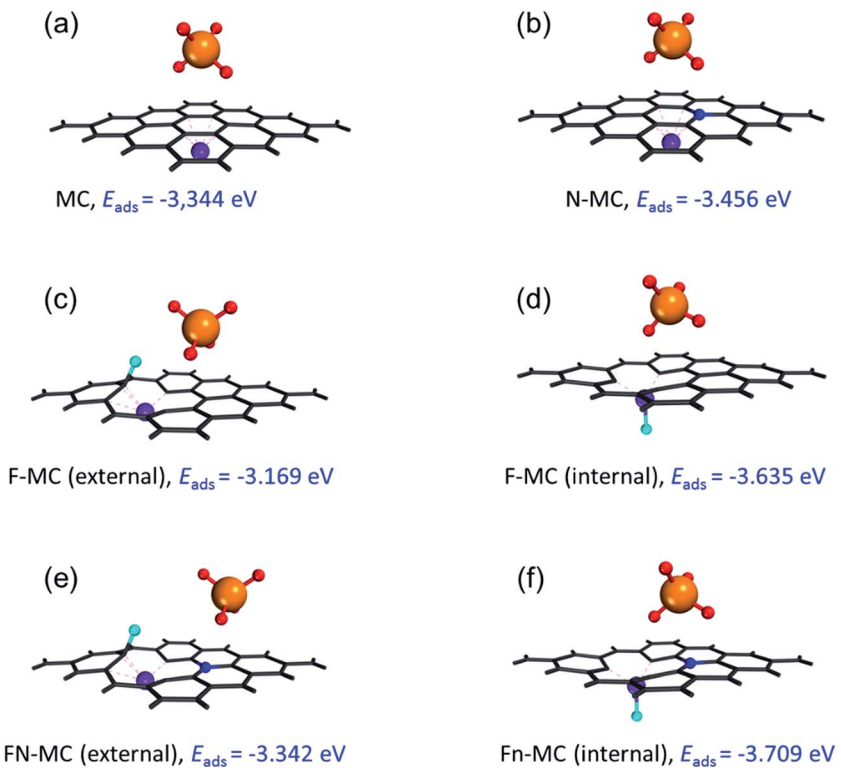

Fig. 8 The optimized adsorption configurations for (a) MC⋯CrO_4^{2-}, (b) N-MC⋯CrO_4^{2-}, (c) F-MC (external)⋯CrO_4^{2-} (d) F-MC (internal)⋯CrO_4^{2-}, (e) FN-MC (external)⋯CrO_4^{2-} and (f) FN-MC (internal)⋯CrO_4^{2-}. The red, blue, purple, cyan and orange balls stand for oxygen, nitrogen, iron, fluorine and chromium atoms, respectively.

forms: in the carbon skeleton (F-MC (external)) and the Fe–F (F-MC (internal)).[45,60] Meanwhile, the electrostatic interaction between the negative CrO_4^{2-} cluster and the adsorbent is shown in Fig. S13.† The more negative adsorption energy indicates that the Cr(VI) cluster is more easily adsorbed and the cluster configuration is more stable.[62] The results showed that the adsorption energy for F atoms inside adsorbents is much lower than that of the outside samples, F-MC (external) (−3.169 eV) > F-MC (internal) (−3.635 eV) and FN-MC (external) (−3.342 eV) > FN-MC (internal) (−3.709 eV). The F doped inside is more stable and greatly enhanced the Cr(VI) removal. As shown in Table S7,† the FN-MC-*w*, washed with concentrated HCl to remove the Fe^0 and Fe^{2+} nanoparticles on the surface of the adsorbent, still exhibited a high removal activity. According to the survey on the magnetic adsorbents, the adsorption energy was sequenced as MC (−3.344 eV) > N-MC (−3.456 eV) > F-MC (internal) > FN-MC (internal), which was consistent with the experimental results (Table 2), demonstrating the synergistic influence of the nitrogen and fluorine co-doping on the Cr(VI) removal.

4. Conclusion

In summary, FN-MCs were synthesised through a simple pyrolysis method and used as an adsorbent for Cr(VI) removal. Good performance and stability of the heteroatom doped adsorbent were achieved, which will essentially reduce the cost of its practical application. Negative density charge on the adsorbent surface plays a significant role, which was facilitated by the nitrogen and fluorine co-doping. The fluorine and nitrogen dopants on the magnetic carbons had a synergistic effect on the Cr(VI) removal, and adsorption capacities as high as 188.7 mg g^{-1} and 2.28 mg m^{-2} in neutral solution and 740.7 mg g^{-1} and 8.96 mg m^{-2} in acid solution were obtained. Graphitic N and heteroatoms at defects, edges or vacancies are the most important active sites for the Cr(VI) removal. The results presented herein provide a new approach for the development of magnetic adsorbents for environmental remediation. In addition, carbon based nanocomposites similar to that reported in the current work may also find great potential applications, such as electromagnetic,[72–74] structural,[75–77] thermochromic,[78] sensory,[79–81] and conductive[82,83] fields.

Conflicts of interest

There are no conflicts to declare.

Acknowledgements

This project was financially supported through the start-up fund of University of Tennessee, National Natural Science Foundation of China (No. 21503082), Science and Technology Program of Guangzhou City (No. 201804010112), State Key Laboratory of Hydraulic Engineering Simulation and Safety (No. HESS-1401) and China Postdoctoral Science Foundation Grant (No. 2018M633053).

References

1 Z. Zhou, X. P. Gao, J. Yan, D. Y. Song and M. Morinaga, *J. Phys. Chem. B*, 2004, **108**, 9023–9026.
2 Y. Wang, X. C. Wang and M. Antonietti, *Angew. Chem., Int. Ed.*, 2012, **51**, 68–89.
3 K. P. Gong, F. Du, Z. H. Xia, M. Durstock and L. M. Dai, *Science*, 2009, **323**, 760–764.
4 A. Thomas, A. Fischer, F. Goettmann, M. Antonietti, J. O. Muller, R. Schlögl and J. M. Carlsson, *J. Mater. Chem.*, 2008, **18**, 4893–4908.
5 Y. Li, S. Zhu, Q. Liu, Z. Chen, J. Gu, C. Zhu, T. Lu, D. Zhang and J. Ma, *Water Res.*, 2013, **47**, 4188–4197.
6 A. Chen, Y. Yu, Y. Zhang, T. Xing, Y. Wang, Y. Zhang and J. Zhang, *J. Hazard. Mater.*, 2014, **279**, 280–288.
7 G. Yu, Y. Lu, J. Guo, M. Patel, A. Bafana, X. Wang, B. Qiu, C. Jeffryes, S. Wei, Z. Guo and E. K. Wujcik, *Adv. Compos. Mater.*, 2018, **1**, 56–78.
8 W. Qi and D. Su, *ACS Catal.*, 2014, **4**, 3212–3218.
9 J. Zhang, X. Liu, R. Blume, A. Zhang, R. Schlögl and D. S. Su, *Science*, 2008, **322**, 73–77.
10 H. Yu, F. Peng, J. Tan, X. W. Hu, H. J. Wang, J. A. Yang and W. X. Zheng, *Angew. Chem., Int. Ed.*, 2011, **50**, 3978–3982.
11 Y. Cao, H. Yu, J. Tan, F. Peng, H. Wang, J. Li, W. Zheng and N.-B. Wong, *Carbon*, 2013, **57**, 433–442.
12 J. Zhou, J. Lian, L. Hou, J. Zhang, H. Gou, M. Xia, Y. Zhao, T. A. Strobel, L. Tao and F. Gao, *Nat. Commun.*, 2015, **6**, 8503.
13 Y. Cao, J. Huang, Y. Li, S. Qiu, J. Liu, A. Khasanov, M. A. Khan, D. P. Young, F. Peng, D. Cao, X. Peng, K. Hong and Z. Guo, *Carbon*, 2016, **109**, 640–649.
14 Y. Cao, J. Huang, X. Peng, D. Cao, A. Galaska, S. Qiu, J. Liu, M. A. Khan, D. P. Young, J. E. Ryu, H. Feng, N. Yerra and Z. Guo, *Carbon*, 2017, **115**, 503–514.
15 A. Modi, B. Bhaduri and N. Verma, *Ind. Eng. Chem. Res.*, 2015, **54**, 5172–5178.
16 P. Suksabye, A. Nakajima, P. Thiravetyan, Y. Baba and W. Nakbanpote, *J. Hazard. Mater.*, 2009, **161**, 1103–1108.
17 L. C. Hsu, S. L. Wang, Y. C. Lin, M. K. Wang, P. N. Chiang, J. C. Liu, W. H. Kuan, C. C. Chen and Y. M. Tzou, *Environ. Sci. Technol.*, 2010, **44**, 6202–6208.
18 Z. Wei, R. Xing, X. Zhang, S. Liu, H. Yu and P. Li, *ACS Appl. Mater. Interfaces*, 2013, **5**, 598–604.
19 B. Qiu, H. Gu, X. Yan, J. Guo, Y. Wang, D. Sun, Q. Wang, M. Khan, X. Zhang, B. L. Weeks, D. P. Young, Z. Guo and S. Wei, *J. Mater. Chem. A*, 2014, **2**, 17454–17462.
20 B. Krishna, D. Murty and B. J. Prakash, *Appl. Clay Sci.*, 2001, **20**, 65–71.
21 A. M. Yusof and N. A. N. N. Malek, *J. Hazard. Mater.*, 2009, **162**, 1019–1024.
22 D. Kratochvil, P. Pimentel and B. Volesky, *Environ. Sci. Technol.*, 1998, **32**, 2693–2698.
23 A. Szabó, D. Gournis, M. A. Karakassides and D. Petridis, *Chem. Mater.*, 1998, **10**, 639–645.
24 H. Tamai, T. Kakii, Y. Hirota, T. Kumamoto and H. Yasuda, *Chem. Mater.*, 1996, **8**, 454–462.

25 B. Qiu, Y. Wang, D. Sun, Q. Wang, X. Zhang, B. L. Weeks, R. O'Connor, X. Huang, S. Wei and Z. Guo, *J. Mater. Chem. A*, 2015, **3**, 9817–9825.
26 J. H. Zhu, H. B. Gu, J. Guo, M. J. Chen, H. G. Wei, Z. P. Luo, H. A. Colorado, N. Yerra, D. Ding, T. C. Ho, N. Haldolaarachchige, J. Hopper, D. P. Young, Z. H. Guo and S. Y. Wei, *J. Mater. Chem. A*, 2014, **2**, 2256–2265.
27 I. L. Shashkova, A. I. Rat'ko and N. V. Kitikova, *Colloids Surf., A*, 1999, **160**, 207–215.
28 C. X. Xu, B. Qiu, H. B. Gu, X. R. Yang, H. G. Wei, X. H. Huang, Y. R. Wang, D. Rutman, D. M. Cao, S. Bhan, Z. H. Guo and S. Y. Wei, *ECS J. Solid State Sci. Technol.*, 2014, **3**, M1–M9.
29 J. H. Zhu, S. Y. Wei, M. J. Chen, H. B. Gu, S. B. Rapole, S. Pallavkar, T. C. Ho, J. Hopper and Z. H. Guo, *Adv. Powder Technol.*, 2013, **24**, 459–467.
30 J. H. Zhu, R. Sadu, S. Y. Wei, D. H. Chen, N. Haldolaarachchige, Z. P. Luo, J. A. Gomes, D. P. Young and Z. H. Guo, *ECS J. Solid State Sci. Technol.*, 2012, **1**, M1–M5.
31 K. Gong, Q. Hu, Y. Xiao, X. Cheng, H. Liu, N. Wang, B. Qiu and Z. Guo, *J. Mater. Chem. A*, DOI: 10.1039/c8ta03066a, in press.
32 K.-Y. Shin, J.-Y. Hong and J. Jang, *J. Hazard. Mater.*, 2011, **190**, 36–44.
33 T. K. Rahul and N. Sandhyarani, *Nanoscale*, 2015, **7**, 18259–18270.
34 S. G. Peera, A. K. Sahu, A. Arunchander, S. D. Bhat, J. Karthikeyan and P. Murugan, *Carbon*, 2015, **93**, 130–142.
35 S. Jiang, Y. Sun, H. Dai, J. Hu, P. Ni, Y. Wang, Z. Li and Z. Li, *Nanoscale*, 2015, **7**, 10584–10589.
36 X. Sun, P. Song, Y. Zhang, C. Liu, W. Xu and W. Xing, *Sci. Rep.*, 2013, **3**, 2505.
37 G. Jing, Z. Zhou, L. Song and M. Dong, *Desalination*, 2011, **279**, 423–427.
38 W.-B. Zhang, M. Deng, C.-X. Sun and S.-B. Wang, *Ind. Eng. Chem. Res.*, 2014, **53**, 333–339.
39 B. Delley, *J. Chem. Phys.*, 2000, **113**, 7756–7764.
40 J. P. Perdew, K. Burke and M. Ernzerhof, *Phys. Rev. Lett.*, 1996, **77**, 3865–3868.
41 B. Delley, *Phys. Rev. B: Condens. Matter Mater. Phys.*, 2002, **66**, 155125.
42 S. Grimme, *J. Comput. Chem.*, 2006, **27**, 1787–1799.
43 Z. Y. Sun, L. Zhang, F. Dang, Y. Liu, Z. Y. Fei, Q. Shao, H. Lin, J. Guo, L. C. Xiang, N. Yerra and Z. H. Guo, *CrystEngComm*, 2017, **19**, 3288–3298.
44 A. Klamt and G. Schuurmann, *J. Chem. Soc., Perkin Trans. 2*, 1993, 799–805, DOI: 10.1039/p29930000799.
45 H. Ming, J. Ming, W.-J. Kwak, W. Yang, Q. Zhou, J. Zheng and Y.-K. Sun, *Electrochim. Acta*, 2015, **169**, 291–299.
46 Y. H. Cao, H. Yu, J. Tan, F. Peng, H. J. Wang, J. Li, W. X. Zheng and N.-B. Wong, *Carbon*, 2013, **57**, 433–442.
47 S. Maldonado, S. Morin and K. J. Stevenson, *Carbon*, 2006, **44**, 1429–1437.
48 C. L. Chen, J. Zhang, B. S. Zhang, C. L. Yu, F. Peng and D. S. Su, *Chem. Commun.*, 2013, **49**, 8151–8153.
49 G. Panomsuwan, N. Saito and T. Ishizaki, *J. Mater. Chem. A*, 2015, **3**, 9972–9981.
50 H. Geng, Q. Zhou, Y. Pan, H. Gu and J. Zheng, *Nanoscale*, 2014, **6**, 3889–3894.
51 J. Giraudet, C. Delabarre, K. Guérin, M. Dubois, F. Masin and A. Hamwi, *J. Power Sources*, 2006, **158**, 1365–1372.
52 L. S. Zhong, J. S. Hu, H. P. Liang, A. M. Cao, W. G. Song and L. J. Wan, *Adv. Mater.*, 2006, **18**, 2426–2431.
53 J. Huang, Y. Cao, Q. Shao, X. Peng and Z. Guo, *Ind. Eng. Chem. Res.*, 2017, **56**, 10689–10701.
54 C. Luo, Z. Tian, B. Yang, L. Zhang and S. Yan, *Chem. Eng. J.*, 2013, **234**, 256–265.
55 J. Wang, K. Pan, Q. He and B. Cao, *J. Hazard. Mater.*, 2013, **244–245**, 121–129.
56 B. Qiu, C. Xu, D. Sun, H. Wei, X. Zhang, J. Guo, Q. Wang, D. Rutman, Z. Guo and S. Wei, *RSC Adv.*, 2014, **4**, 29855.
57 B. Qiu, J. Guo, X. Zhang, D. Sun, H. Gu, Q. Wang, H. Wang, X. Wang, X. Zhang, B. L. Weeks, Z. Guo and S. Wei, *ACS Appl. Mater. Interfaces*, 2014, **6**, 19816–19824.
58 J. H. Zhu, S. Y. Wei, H. B. Gu, S. B. Rapole, Q. Wang, Z. P. Luo, N. Haldolaarachchige, D. P. Young and Z. H. Guo, *Environ. Sci. Technol.*, 2012, **46**, 977–985.
59 H. Wang, X. Yuan, Y. Wu, X. Chen, L. Leng, H. Wang, H. Li and G. Zeng, *Chem. Eng. J.*, 2015, **262**, 597–606.
60 J. T. Robinson, J. S. Burgess, C. E. Junkermeier, S. C. Badescu, T. L. Reinecke, F. K. Perkins, M. K. Zalalutdniov, J. W. Baldwin, J. C. Culbertson and P. E. Sheehan, *Nano Lett.*, 2010, **10**, 3001–3005.
61 Y. Cao, B. Li, G. Zhong, Y. Li, H. Wang, H. Yu and F. Peng, *Carbon*, 2018, **133**, 464–473.
62 H. Valencia, A. Gil and G. Frapper, *J. Phys. Chem. C*, 2010, **114**, 14141–14153.
63 J. Wang, S. Xu, Y. Wang, R. Cai, C. Lv, W. Qiao, D. Long and L. Ling, *RSC Adv.*, 2014, **4**, 16224–16232.
64 A. El-Sikaily, A. E. Nemr, A. Khaled and O. Abdelwehab, *J. Hazard. Mater.*, 2007, **148**, 216–228.
65 S. Zhang, X. Wang, J. Li, T. Wen, J. Xu and X. Wang, *RSC Adv.*, 2014, **4**, 63110–63117.
66 J. Cao and W.-X. Zhang, *J. Hazard. Mater.*, 2006, **132**, 213–219.
67 W. S. Choi, H. M. Yang, H. Y. Koo, H.-J. Lee, Y. B. Lee, T. S. Bae and I. C. Jeon, *Adv. Funct. Mater.*, 2010, **20**, 820–825.
68 M. Avila, T. Burks, F. Akhtar, M. Gothelid, P. C. Lansaker, M. S. Toprak, M. Muhammed and A. Uheida, *Chem. Eng. J.*, 2014, **245**, 201–209.
69 X.-F. Sun, C. Liu, Y. Ma, S.-G. Wang, B.-Y. Gao and X.-M. Li, *Colloids Surf., B*, 2011, **82**, 456–462.
70 S. Deng and R. Bai, *J. Colloid Interface Sci.*, 2004, **280**, 36–43.
71 X.-J. Hu, J.-S. Wang, Y.-G. Liu, X. Li, G.-M. Zeng, Z.-L. Bao, X.-X. Zeng, A.-W. Chen and F. Long, *J. Hazard. Mater.*, 2011, **185**, 306–314.
72 K. Sun, P. Xie, Z. Wang, T. Su, Q. Shao, J. Ryu, X. Zhang, J. Guo, A. Shankar, J. Li, R. Fan, D. Cao and Z. Guo, *Polymer*, 2017, **125**, 50–57.
73 C. Cheng, R. Fan, Z. Wang, Q. Shao, X. Guo, P. Xie, Y. Yin, Y. Zhang, L. An, Y. Lei, J. E. Ryu, A. Shankar and Z. Guo, *Carbon*, 2017, **125**, 103–112.

74 K. Zhang, G. Li, L. Feng, N. Wang, J. Guo, K. Sun, K. Yu, J. Zeng, T. Li, Z. Guo and M. Wang, *J. Mater. Chem. C*, 2017, **5**, 9359–9369.
75 C. Wang, M. Zhao, J. Li, J. Yu, S. Sun, S. Ge, X. Guo, F. Xie, B. Jiang, E. Wujcik, Y. Huang, N. Wang and Z. Guo, *Polymer*, 2017, **131**, 263–271.
76 Z. Wu, S. Gao, L. Chen, D. Jiang, Q. Shao, B. Zhang, Z. Zhai, C. Wang, M. Zhao, Y. Ma, X. Zhang, L. Weng, M. Zhang and Z. Guo, *Macromol. Chem. Phys.*, 2017, **218**, 1700357.
77 Z. Wu, H. Cui, L. Chen, D. Jiang, L. Weng, Y. Ma, X. Li, X. Zhang, H. Liu, N. Wang, J. Zhang, Y. Ma, M. Zhang, Y. Huang and Z. Guo, *Compos. Sci. Technol.*, 2018, **164**, 195–203.
78 B. Zhou, Y. Li, K. Dai, G. Zheng, C. Liu, Y. Ma, J. Zhang, N. Wang, C. Shen and Z. Guo, *J. Mater. Chem. C*, DOI: 10.1039/c8tc01779d, in press.
79 H. Liu, Y. Li, K. Dai, G. Zheng, C. Liu, C. Shen, X. Yan, J. Guo and Z. Guo, *J. Mater. Chem. C*, 2016, **4**, 157–166.
80 H. Liu, M. Dong, W. Huang, J. Gao, K. Dai, J. Guo, G. Zheng, C. Liu, C. Shen and Z. Guo, *J. Mater. Chem. C*, 2017, **5**, 73–83.
81 C. Hu, Z. Li, J. Gao, K. Dai, G. Zheng, C. Liu, C. Shen, H. Song and Z. Guo, *J. Mater. Chem. C*, 2017, **5**, 2318–2328.
82 H. Liu, W. Huang, X. Yang, K. Dai, G. Zheng, C. Liu, C. Shen, X. Yan, J. Guo and Z. Guo, *J. Mater. Chem. C*, 2016, **4**, 4459–4469.
83 X. Guan, G. Zheng, K. Dai, C. Liu, X. Yan, C. Shen and Z. Guo, *ACS Appl. Mater. Interfaces*, 2016, **8**, 14150–14159.